Published in final edited form as:
Phys Rev Lett. 2009 March 27; 102(12): 126804.

Softening of the Radial Breathing Mode in Metallic Carbon Nanotubes

H. Farhat[1], **K. Sasaki**[2], **M. Kalbac**[3], **M. Hofmann**[4], **R. Saito**[5], **M. S. Dresselhaus**[4,6], and **J. Kong**[4]

[1]Department of Materials Science and Engineering, MIT, Cambridge Massachusetts 02139, USA

[2]Department of Quantum Matter, Graduate School of Advanced Sciences of Matter, Hiroshima University, Higashi-Hiroshima 739-8530, Japan

[3]J. Heyrovský Institute of Physical Chemistry, Academy of Sciences of the Czech Republic, V.V.i., Dolejskova 3, CZ-18223 Prague 8, Czech Republic

[4]Department of Electrical Engineering and Computer Science, MIT, Cambridge Massachusetts 02139, USA

[5]Department of Physics, Tohoku University, Sendai, 980-8578, Japan

[6]Department of Physics, MIT, Cambridge Massachusetts 02139, USA

Abstract

The softening of the radial breathing mode (RBM) of metallic single walled carbon nanotubes (m-SWNTs) due to electron-phonon coupling has been studied by observing the Fermi level (ε_F) dependence of the RBM Raman peak. *In situ* Raman spectra were obtained from several individual m-SWNTs while varying ε_F electrochemically. The RBM frequency of an intrinsic m-SWNT is shown to be down-shifted relative to highly doped tubes by ~2 cm^{-1}. The down-shift is greatest for small diameter and small chiral angle SWNTs. Most tubes show no change in RBM linewidth. A comparison is drawn between the RBM and the G band (A_{LO} phonon) with respect to the ε_F dependence of their frequencies and linewidths.

Electron-phonon (*e*-ph) interactions govern many aspects of the physical properties of materials. In graphene and single walled carbon nanotubes (SWNTs), the coupling between electrons and the in-plane C-C stretching optical phonon modes (*G*-band phonons) influences the phonon structure [1,2], electrical transport [3], and optical transition properties of these materials [4]. Thus, significant effort has been devoted to this subject recently. Another phonon mode of interest in SWNTs is the isotropic radial deformation of the nanotube called the radial breathing mode (RBM). This optical phonon is solely the result of the one-dimensional tubular structure of SWNTs and its deformations are very different from those of the optical stretching modes that are common to all other graphitic materials. *e*-ph coupling of the RBM is important because it provides a new scattering channel for electrons that is absent in higher dimensional forms of carbon. Being a low energy optical phonon, the RBM could be a significant scatterer of low energy electrons such as in electrical transport at low biases [5].

In metallic SWNTs (m-SWNTs) *e*-ph coupling can be especially strong because a wide range of phonon energies is able to resonantly excite electrons across the linear electronic bands. Phonons that effectively couple to excitations near the Fermi surface experience lifetime broadening and energy renormalization [1,2]. This phenomenon is typically investigated by studying how the phonon energy and lifetime evolve as a function of the Fermi energy, ε_F. For the G^- Raman peak of a m-SWNT, the observed up-shift and

narrowing of the peak with doping has helped clarify the origin of the metallic G-band line shape and the role of electronic excitations in the softening of the A_{LO} phonon at ε_F for the neutral m-SWNT [6]. A recent theoretical treatment of the ε_F dependence of the RBM predicts a similar, albeit weaker, softening of the RBM phonon with a significantly larger chiral angle dependence [7]. Because the RBM energy is so much smaller than the G band, the e-ph coupling is expected to be much more sensitive to the fine structure of the electronic bands near the Dirac point where the valence and conduction bands touch. An experimental study of the softening of the RBM frequency in m-SWNTs is therefore important to clarify the structure-dependent e-ph coupling phenomena associated with the RBM phonon.

In this Letter we present a careful analysis of the frequency ω_{RBM} and linewidth γ_{RBM} of the RBM of individual SWNTs as a function of the electrochemical gating potential V_g. We observe an increase in frequency when the nanotube is doped with either electrons or holes. Our experimental results show a diameter (d_t) and chiral angle (θ) dependence of the ω_{RBM} softening.

We use a transparent polymer electrolyte (PEO/$LiClO_4$) to electrochemically dope m-SWNTs. Long, gas flow aligned SWNTs are grown by chemical vapor deposition and then contacted by a Cr/Au electrode to form the working electrode of the electrochemical cell. The SWNTs are typically several hundred microns long and are separated from each other by 20–50 μm. A Pt counter electrode is controlled by a Princeton Applied Research 283 potentiostat to vary the potential (V_g) of an Ag pseudo-reference electrode with respect to the SWNTs [8]. Raman measurements are made through the transparent electrolyte. The nanotube metallicity is determined by placing ω_{RBM} and the excitation energy E_{laser} on a Kataura plot, and by observing a broadening and shift of the G band [6]. The m-SWNTs under study are either isolated or in small bundles of two or three SWNTs. However, only one SWNT contributes to the signal for these measurements.

Figure 1(a) shows the RBM spectrum of a m-SWNT at several values of V_g. Here, a positive (negative) V_g corresponds to electron (hole) doping. A subtle up-shift of 2 cm^{-1} for both (±) polarities of V_g is observed. Changes in ω_{RBM} are more evident after fitting the peaks, whereby the fit gives both ω_{RBM} and the FWHM linewidth γ_{RBM} versus V_g, shown in Figs. 1(b) and 1(c), respectively. We use a Voigt profile to deconvolute the instrumental broadening from the Lorentzian linewidth of the RBM peak. The ω_{RBM} of the m-SWNT shown in Fig. 1(b) makes an almost symmetric "V" shape about $V_g = 0$. Previous studies suggest that environmental effects such as the van der Waals interaction of the SWNT with the substrate or surrounding solution may modify ω_{RBM} [9]. The latter effect presumably only contributes to a constant background with respect to V_g. The large drop in the peak intensity observed with increasing V_g may be caused by a change in the resonance condition. Because of the loss in peak intensity with increasing V_g, we are only able to follow ω_{RBM} (V_g) for those m-SWNTs that have strong signals, which biases our sample set towards tubes with small θ values [7]. These m-SWNTs all exhibit a similar characteristic ω_{RBM} (V_g) behavior. Meanwhile, the RBM peak for a semiconducting SWNT (s-SWNT) shows no appreciable change in ω_{RBM} (V_g) as a function of V_g, as, for example, shown in the inset of Fig. 1(b). It is thus clear that the behavior in Fig. 1(b) is an effect specific to m-SWNTs.

The behavior of ω_{RBM} for m-SWNTs can be understood by considering that, like the G-band phonons, the RBM is also an optical phonon capable of exciting vertical electron-hole (e-h) pairs across the linear k valence and conduction bands of the m-SWNT near the K (or K') point. If the e-ph matrix element for such transitions is nonzero, these scattering events contribute to renormalizing the phonon energy and decreasing its lifetime. As illustrated in

the inset of Fig. 1(a), the Pauli exclusion principle limits the available *e-h* pair transitions to those satisfying $E_{e\text{-}h} > 2|\varepsilon_F|$, thus giving rise to the V_g dependence of ω_{RBM}. As ε_F is shifted away from the Dirac point, the number of excitations contributing to the *dressed* RBM phonon is reduced and ω_{RBM} approaches the frequency of the *bare* RBM phonon [7].

In Fig. 2 we compare the ε_F dependence of the G^- peak (A_{LO} phonon) to ω_{RBM} of a m-SWNT which we tentatively assign as a (13,4) SWNT ($\omega_{\mathrm{RBM}} = 193\ \mathrm{cm}^{-1}$, $E_{\mathrm{laser}} = 1.91$ eV). We see a striking resemblance between the V_g dependence of ω_{G^-} and that of ω_{RBM}, with both peaks displaying a minimum in frequency around $V_g = 0$. However, the γ_{RBM} behavior of the two peaks is quite different with the RBM peak showing no noticeable broadening in contrast to the 60 cm^{-1} broadening of the G^- peak. The lack of broadening for the RBM indicates a negligible resonant decay of the RBM into an *e-h* pair.

To understand why the RBM is down-shifted but not broadened, it is instructive to draw comparisons to the *e*-ph coupling of the optical phonons that contribute to the *G* band of graphene, m-SWNTs and s-SWNTs, which have recently been studied in great detail [6,10-13]. In m-SWNTs, the LO phonon (with energy 0.2 eV) is able to create real and virtual *e-h* pairs across the linear electronic bands, resulting in the strong broadening and downshift in frequency characteristic of the metallic G^- peak as shown in Fig. 2. Similarly, in graphene, the *G*-band phonons are both broadened and down-shifted because they couple to *e-h* excitations near the Dirac point. In the case of s-SWNTs, the optical phonons do not have sufficient energy to excite *e-h* pair excitations across the large electronic energy gap. However, these optical phonons can still create virtual excitations which contribute to the down-shift of the phonon frequency. Since there is no decay into real states, there is no linewidth broadening and the frequency shift is modest compared to that of m-SWNTs, as recently verified in experiments [13,14].

Since $\hbar\omega_{\mathrm{RBM}}$ is a small fraction of the LO/TO phonon energies, the *e-h* excitations for the RBM occur much closer to the Dirac point. On this energy scale a very small energy gap, such as the curvature-induced minigap, becomes significant. The latter, given by $E_{\mathrm{gap}}=(A/d_t^2)\times\cos(3\theta)$, is greatest for zigzag and absent for armchair m-SWNTs. The value of A is about 60 meV based on an extended tight-binding model [7]. From the perspective of the RBM phonon, the electronic bands of small diameter zigzag m-SWNTs with $E_{\mathrm{gap}} > \hbar\omega_{\mathrm{RBM}}$ appear semiconductinglike. Only the armchair SWNTs have truly metallic bands when close to the Dirac point. Indeed, for the (13,4) SWNT shown in Fig. 2, $E_{\mathrm{gap}} = 32$ meV ($d_t = 1.2$ nm, $\theta = 13°$) exceeds the $\hbar\omega_{\mathrm{RBM}}$ (24 meV) and hence no linewidth broadening is expected.

In Fig. 3 we show ω_{RBM} for the (13,4) nanotube calculated from the effective mass theory in [7], which also predicts no change in γ_{RBM} as a function of ε_F and a ω_{RBM} behavior qualitatively similar to what we observe in our measurements. For a quantitative comparison, we converted the V_g scale of Fig. 2 to an energy scale (bottom axis) using a gate efficiency of $\alpha = 0.24$ (eV/V). The α value is determined by fitting the broadening window of the G^- peak to $\gamma_{G-} = \gamma_o + \gamma_{\mathrm{EPC}}(V_g)$, as shown in Fig. 2(b). Here, γ_{EPC}, the linewidth due to *e*-ph coupling, is given by Eq. (29) of [1]. The V_g independent contributions to the linewidth are included in γ_o which is taken as 10 cm^{-1} based on our experimental results. Comparing Fig. 2(c) with Fig. 3 within the same ε_F range, we see that the experimental shift of ω_{RBM} is approximately a factor of 2 smaller than that predicted.

It is important to know in what d_t range the softening of ω_{RBM} becomes significant. The down-shift in ω_{RBM} is greatest in smaller d_t m-SWNTs as seen in Fig. 4, which plots the observed frequency down-shift relative to $V_g = V_0 + 1\,V$ (black) and relative to $V_g = V_0 - 1\,V$ [gray (red)] as a function of $1/d_t$ for several m-SWNTs, where V_0 is the gate voltage

where the minimum in frequency occurs. The e-ph matrix element and hence the frequency shift $\Delta\omega_{\mathrm{RBM}}$ at a constant V_g is expected to be linear in $1/d_t$ [7]. The experimental data increase monotonically versus $1/d_t$ with some variation that we attribute to the expected θ dependence of ω_{RBM} [7]. Note that the shift on the negative gate side is in most cases greater than it is on the positive side. We attribute the mild asymmetry with respect to the sign of V_g to the C-C bond softening (stiffening) due to charging the lattices with electrons (holes). There may also be a difference in the gating efficiency for $\pm V_g$.

To further explore the θ dependence of ω_{RBM} we have measured the V_g dependence of three consecutive m-SWNTs from the $2n + m = 24$ family, namely, (11,2), (10,4), and (9,6) as shown in Fig. 5. For a given V_g, the magnitude of the measured $\Delta\omega_{\mathrm{RBM}}$ decreases from the (11,2) to the (9,6) nanotube. This is in agreement with the predicted θ dependence of the down-shift in ω_{RBM} [7]. The e-ph matrix element, given approximately by $\langle e\text{-}h|H_{e\text{-ph}}|\mathrm{RBM}\rangle = g(|s_z|/d_t)\cos(3\theta)$, where g is the off-site e-ph coupling constant and s_z is the radial displacement, is greatest for the zigzag m-SWNT and approaches zero for the armchair m-SWNT [7]. Consequently the zigzag RBM is expected to exhibit the largest frequency shift but no broadening, while the armchair RBM should show neither a change in ω_{RBM} nor in γ_{RBM}. An intermediate chiral m-SWNT could be expected to exhibit both a frequency shift and a broadening. Within the $2n + m = 24$ family, only the (9,6) and (8,8) tubes have a RBM phonon which is greater in energy than the curvature-induced band gap. As shown in Ref. [7], the (9,6) tube is expected to exhibit a broadening $\Delta\gamma = 2\ \mathrm{cm}^{-1}$ and a negligible frequency shift at 300 K. However, we observe a small frequency shift and no change in linewidth. On the other hand, the (10,4) SWNT is not expected to exhibit any broadening, but we observe a possible small broadening of $\Delta\gamma = 1\ \mathrm{cm}^{-1}$. Besides these deviations, the overall measured d_t and θ dependences of the ω_{RBM} down-shift are in good qualitative agreement with Ref. [7].

It should be noted that the energy gaps for the (9,6) and (10,4) nanotubes are only 7 meV below and 15 meV above their RBM phonon energies, respectively. The ω_{RBM} and γ_{RBM} of m-SWNTs are predicted to depend strongly on the position of the cutting line with respect to the K point, as well as on the size of the energy gap with respect to the $\hbar\omega_{\mathrm{RBM}}$. Small perturbations to the lattice such as strain [15], the displacement of the A_{LO} phonon [16,17], and breaking of mirror symmetry [18] could sufficiently change the electronic structure to alter the ε_F dependence of the RBM peak.

In summary, we have experimentally confirmed that there is a mild softening of the ω_{RBM} of m-SWNTs which can be removed by both positive and negative doping. The magnitude of the down-shift scales with $1/d_t$, and is largest for small θ. The measured ω_{RBM} shifts agree qualitatively with the curvature-dependent softening in Ref. [7]. No gate-induced change in γ_{RBM} is found for most of the SWNTs that we studied, as is expected [7] for small (d_t) SWNTs. Our result shows that chirality dependent corrections to ω_{RBM} are required to better assign the d_t and (n, m) indices for small d_t m-SWNTs, and that environmental doping can be responsible for some of the variability in the observed ω_{RBM}. This work also implies that the role of the RBM in electrical transport and other phonon assisted relaxation processes warrants further investigation.

Acknowledgments

This work is mainly supported by the Materials, Structure and Devices (MSD) Center, one of the five programs in the focus center research program (FCRP), a Semiconductor Research Corporation program. Raman measurements were carried out in the George R. Harrison Spectroscopy Laboratory supported by NSF-CHE 0111370 and NIH-RR02594. M. S.D. was supported by NSF/DMR 07-04197 and R. S. by MEXT Grants (No. 20241023 and No. 16076201).

References

1. Caudal N, et al. Phys Rev B. 2007; 75:115423.
2. Sasaki K, et al. Phys Rev B. 2008; 77:245441.
3. Yao Z, Kane CL, Dekker C. Phys Rev Lett. 2000; 84:2941. [PubMed: 11018981]
4. Chou SG, et al. Phys Rev B. 2005; 72:195415.
5. Perebeinos V, Tersoff J, Avouris P. Phys Rev Lett. 2005; 94:086802. [PubMed: 15783915]
6. Farhat H, et al. Phys Rev Lett. 2007; 99:145506. [PubMed: 17930687]
7. Sasaki K, et al. Phys Rev B. 2008; 78:235405.
8. The gate potential $V_g = -V_e$, where Ve is the electrochemical potential, defined as the potential of the working electrode with respect to the reference electrode.
9. Araujo PT, et al. Phys Rev B. 2008; 77:241403(R).
10. Yan J, Zhang Y, Kim P, Pinczuk A. Phys Rev Lett. 2007; 98:166802. [PubMed: 17501446] Pisana S, et al. Nature Mater. 2007; 6:198. [PubMed: 17293849]
11. Nguyen KT, Gaur A, Shim M. Phys Rev Lett. 2007; 98:145504. [PubMed: 17501287]
12. Wu Y, et al. Phys Rev Lett. 2007; 99:027402. [PubMed: 17678258]
13. Tsang JC, et al. Nature Nanotech. 2007; 2:725.
14. Kalbac M, et al. Nano Lett. 2008; 8:3532. [PubMed: 18798684]
15. Huang MY, et al. Phys Rev Lett. 2008; 100:136803. [PubMed: 18517983]
16. Dubay O, Kresse G, Kuzmany H. Phys Rev Lett. 2002; 88:235506. [PubMed: 12059378]
17. Samsonidze GG, et al. Phys Rev B. 2007; 75:155420.
18. Ouyang M, Huang JL, Cheung CL, Lieber CM. Science. 2001; 292:702. [PubMed: 11326093]

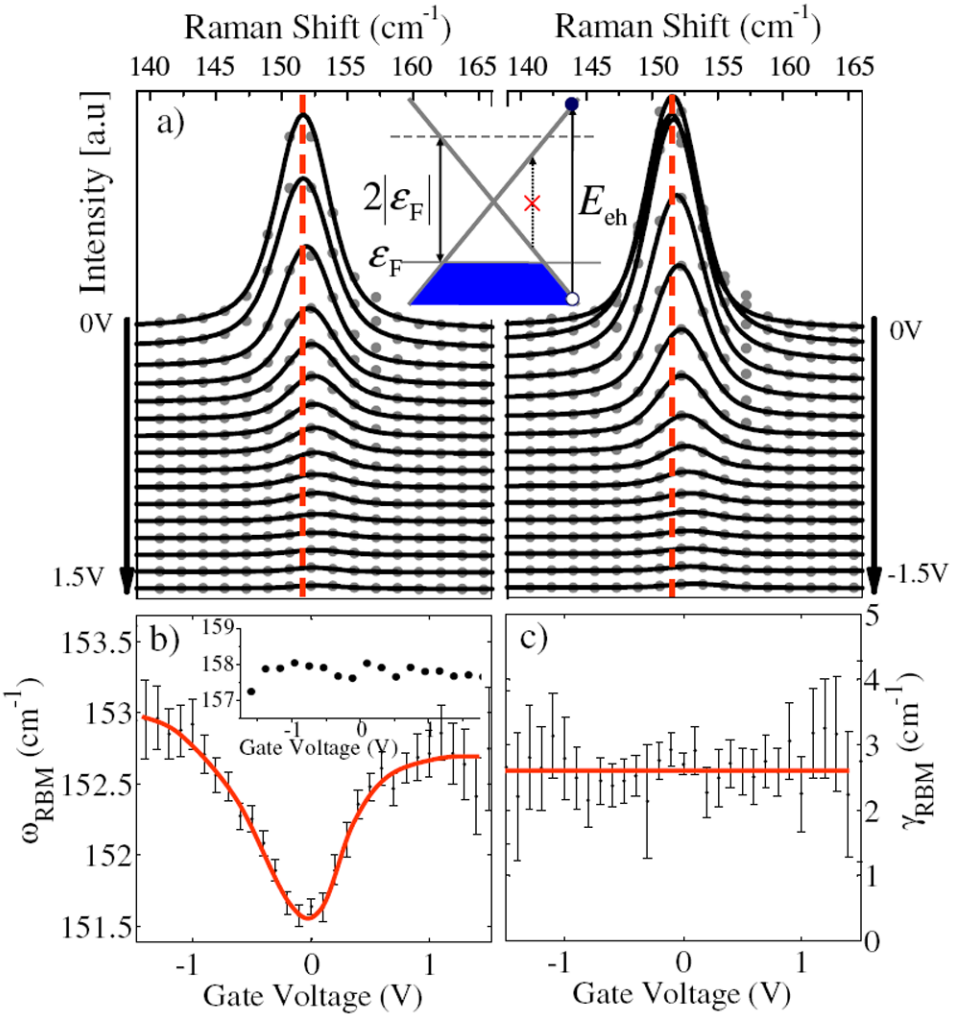

FIG. 1.

(color online). (a) Waterfall plots of the RBM spectra of a m-SWNT at several positive (left-hand panel) and negative (right-hand panel) values of gate potential V_g. To evaluate the ω_{RBM} down-shift we use the vertical red lines as fiduciary marks indicating the peak frequency at $V_g = 0$. The inset of (a) is a schematic band structure of a m-SWNT illustrating the allowed *e-h* transitions. (b) Fitted frequency ω_{RBM} and (c) FWHM linewidth γ_{RBM} values versus V_g. Error bars denote 95% confidence interval. Solid curves guide the eye. The inset of (b) shows the fitted $\omega_{RBM}(V_g)$ for a s-SWNT.

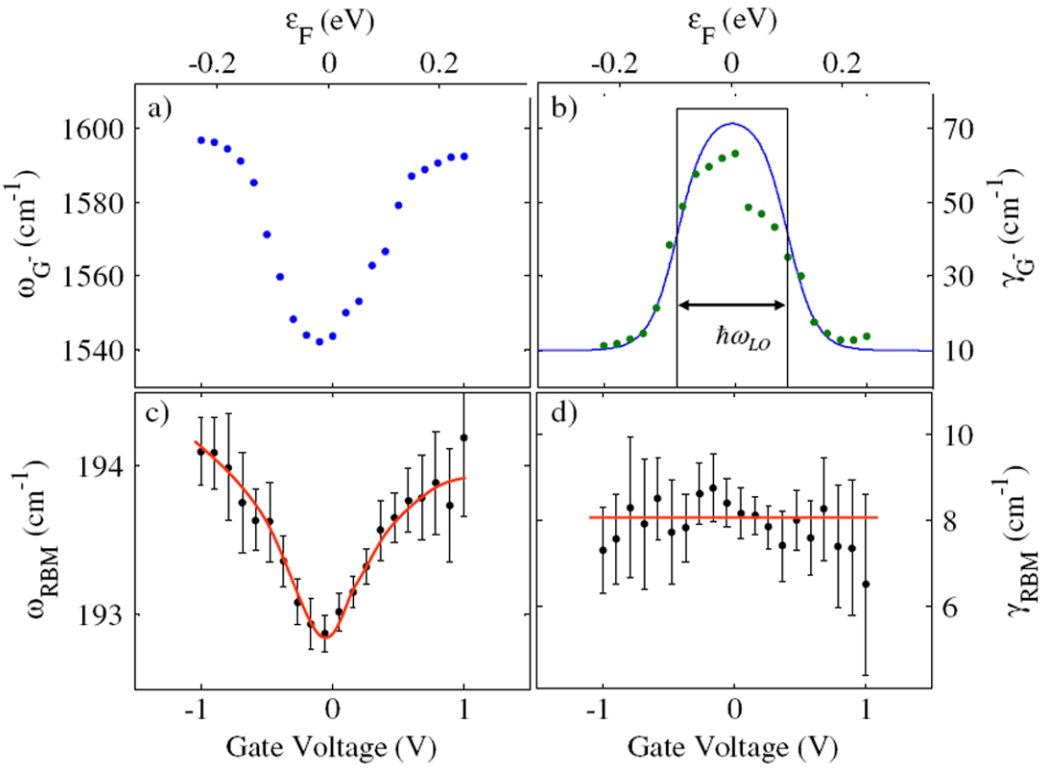

FIG. 2.

(color online). Comparing the G^- and RBM peaks versus V_g for a (13,4) m-SWNT (ω_{RBM} ~ 193 cm^{-1}, E_{laser} = 1.91 eV). (a) the G^- frequency and (b) G^- linewidth versus V_g (bottom axis) and ε_F (top axis). The V_g dependence of the γ_{G^-} is used to estimate the gating efficiency, α = 0.24 eV/V. The box in (b) gives the T = 0 energy range within which the LO phonon can excite real *e-h* pairs. (c) ω_{RBM} and (d) γ_{RBM} for the same m-SWNT.

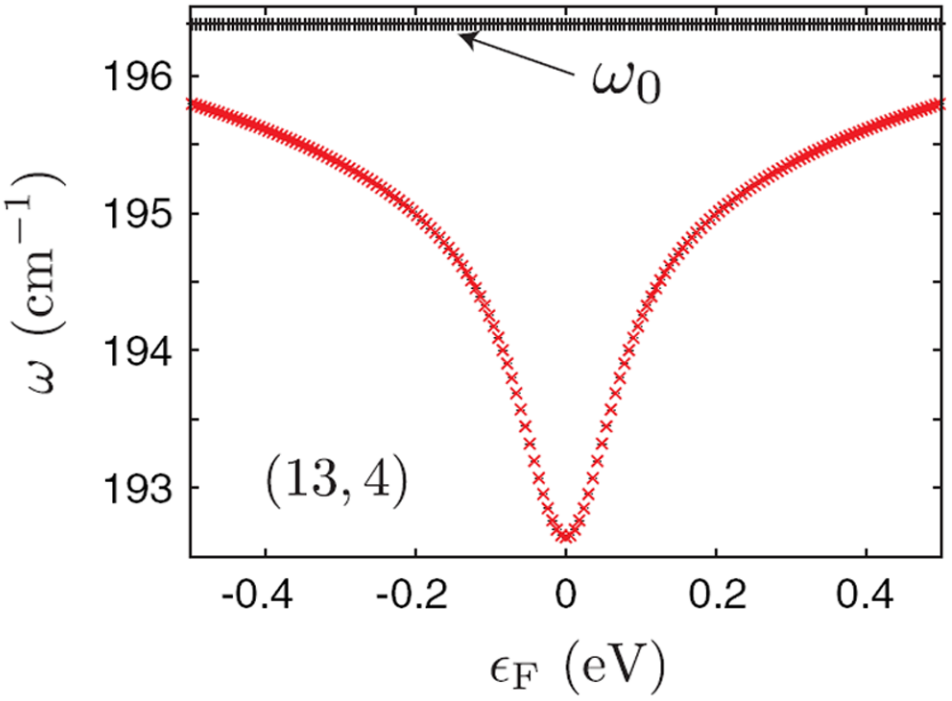

FIG. 3.

(color online). Calculated ω_{RBM} versus ε_F for a (13,4) m-SWNT. For this m-SWNT the *e*-ph coupling contribution to the γ_{RBM} is zero. Black points ω_0 give the *bare* ω_{RBM} and gray (red) points give the corrected ω_{RBM} [7].

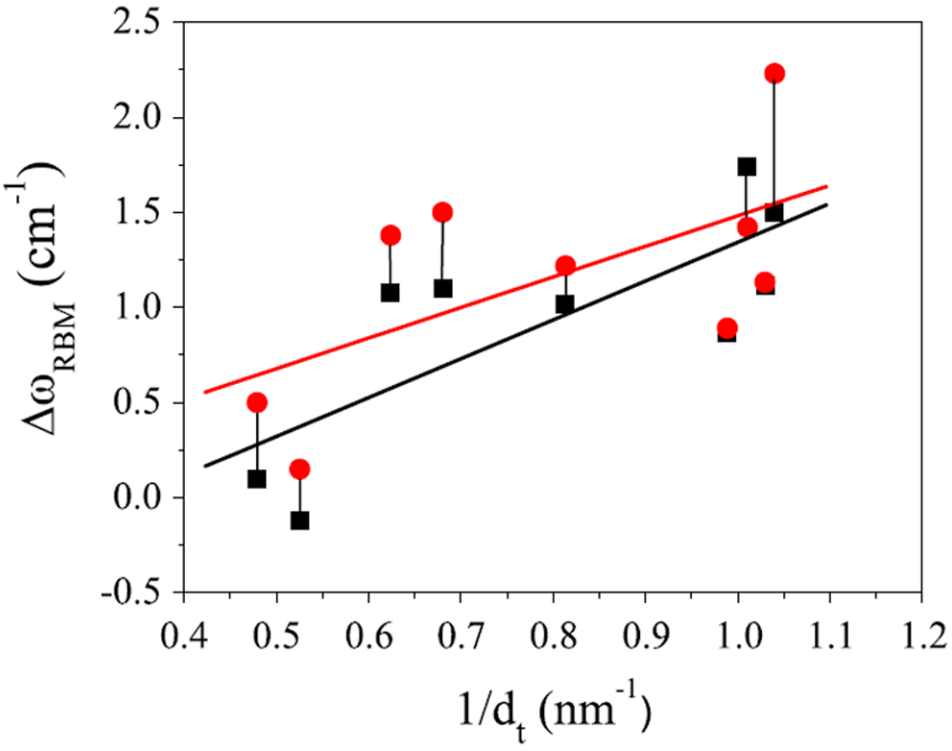

FIG. 4.

(color online). The down-shift $\Delta\omega_{\mathrm{RBM}}$ in ω_{RBM} vs $1/d_t$. Red circles indicate the shift relative to $V_g = V_0 - 1\,V$ (hole doping) and black squares indicate the shift relative to $V_g = V_0 + 1\,V$ (electron doping). Solid lines represent linear fits to the experimental data points.

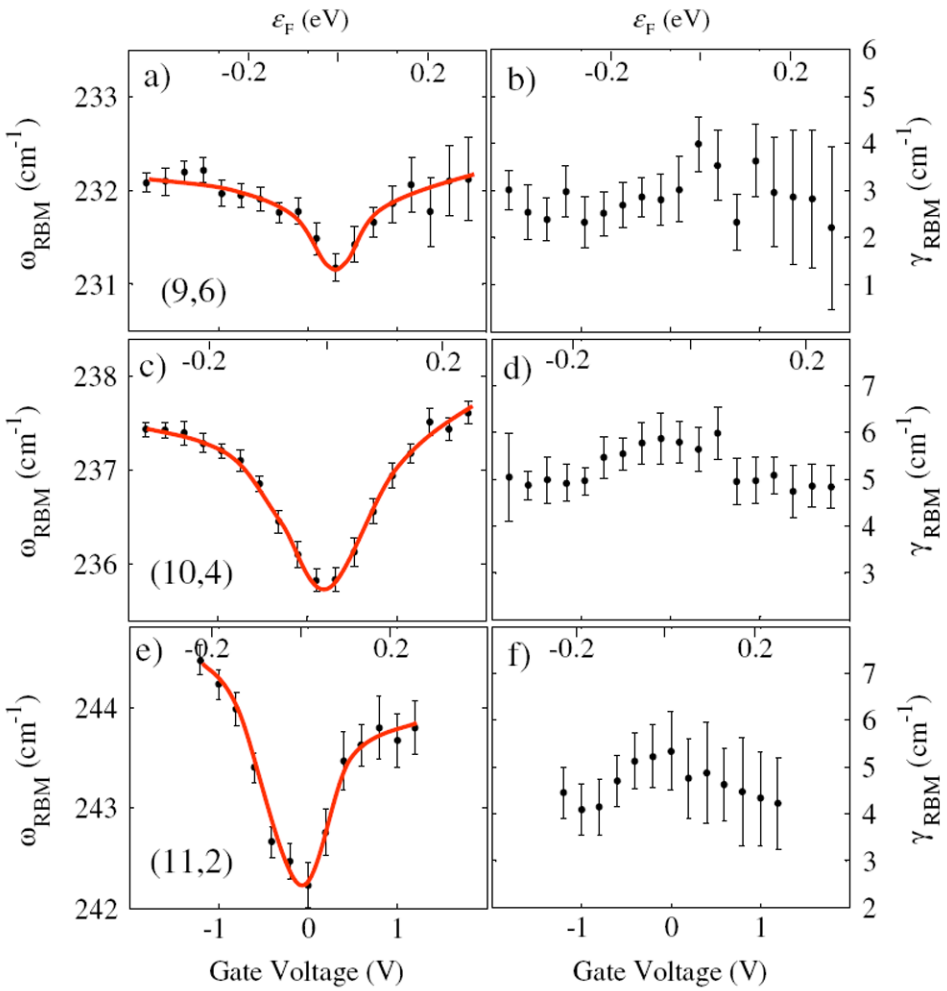

FIG. 5.

(color online). Fitted ω_{RBM} and γ_{RBM} for three m-SWNTs from family $2n + m = 24$. (a),(b) (9,6); (c), (d) (10,4); (e),(f) (11,2). The curvature-induced energy gaps for the three m-SWNTs are 19.3, 41.7, and 60.5 meV, respectively. The energy scale (top axis) is estimated for each m-SWNT as in Fig. 2. Solid red lines are curves to guide the eye.